Journal of Inclusion Phenomena and Macrocyclic Chemistry (2019) 94:155–165
https://doi.org/10.1007/s10847-019-00926-6

ORIGINAL ARTICLE

# Hydrogen-bonded supramolecular metal-imidazolate frameworks: gas sorption, magnetic and UV/Vis spectroscopic properties

**Anas Alrefai[1] · Suvendu Sekhar Mondal[1] · Alexander Wruck[1] · Alexandra Kelling[1] · Uwe Schilde[1] · Philipp Brandt[2] · Christoph Janiak[2] · Sophie Schönfeld[3] · Birgit Weber[3] · Lawrence Rybakowski[4] · Carmen Herrman[4] · Katlen Brennenstuhl[5] · Sascha Eidner[5] · Michael U. Kumke[5] · Karsten Behrens[1] · Christina Günter[6] · Holger Müller[1] · Hans-Jürgen Holdt[1]**

Received: 12 March 2019 / Accepted: 23 May 2019 / Published online: 15 June 2019


## Abstract

By varying reaction parameters for the syntheses of the hydrogen-bonded metal-imidazolate frameworks (HIF) HIF-1 and HIF-2 (featuring 14 Zn and 14 Co atoms, respectively) to increase their yields and crystallinity, we found that HIF-1 is generated in two different frameworks, named as HIF-1a and HIF-1b. HIF-1b is isostructural to HIF-2. We determined the gas sorption and magnetic properties of HIF-2. In comparison to HIF-1a (Brunauer–Emmett–Teller (BET) surface area of 471 $m^2\ g^{-1}$), HIF-2 possesses overall very low gas sorption uptake capacities [BET($CO_2$) surface area = 85 $m^2\ g^{-1}$]. Variable temperature magnetic susceptibility measurement of HIF-2 showed antiferromagnetic exchange interactions between the cobalt(II) high-spin centres at lower temperature. Theoretical analysis by density functional theory confirmed this finding. The UV/Vis-reflection spectra of HIF-1 (mixture of HIF-1a and b), HIF-2 and HIF-3 (with 14 Cd atoms) were measured and showed a characteristic absorption band centered at 340 nm, which was indicative for differences in the imidazolate framework.

**Keywords** Gas-sorption · Ligand design · Magnetic properties · Supramolecular chemistry · Solvothermal synthesis

**Electronic supplementary material** The online version of this article (doi:https://doi.org/10.1007/s10847-019-00926-6) contains supplementary material, which is available to authorized users.

✉ Hans-Jürgen Holdt
holdt@uni-potsdam.de

[1] Institut für Chemie, Anorganische Chemie, Universität Potsdam, Karl-Liebknecht-Straße 24-25, 14476 Potsdam-Golm, Germany

[2] Institut für Anorganische-und Strukturchemie I, Heinrich-Heine-Universität Düsseldorf, Universitätsstraße 1, 40225 Düsseldorf, Germany

[3] Anorganische Chemie IV, Universität Bayreuth, Universitätsstraße 30, NWI, 95447 Bayreuth, Germany

[4] Institut für Anorganische und Angewandte Chemie, Universität Hamburg, Martin-Luther-King-Platz 6, 20146 Hamburg, Germany

[5] Institut für Chemie, Physikalische Chemie, Universität Potsdam, Karl-Liebknecht-Straße 24-25, 14476 Potsdam-Golm, Germany

[6] Institut für Geowissenschaften, Universität Potsdam, Karl-Liebknecht-Straße 24-25, 14476 Potsdam-Golm, Germany

## Introduction

The ability to control the coordination number, and thus geometry, around metal nodes through metal–ligand directed assembly allows construction of predesigned finite and rigid supramolecular building blocks (SBBs). These SBBs must have peripheral coordination sites (e.g., unsaturated metal) and/or peripheral organic functionalities that can either coordinate additional metals not involved in the assembly or act as hydrogen bond donors or acceptors [1, 2].

2-Substitued 4,5-dicyanoimidazole ligands are useful precursors in obtaining by in situ hydrolysis multitopic linkers which can act simultaneously as bridging and capping ligands. Such ligands are necessary for assembling with metal ions to porous hydrogen-bonded metal–organic cubes (MOC) [3–7]. For example, by the reaction of $In(NO_3)_3{\cdot}5H_2O$ with 4,5-dicyanoimidazole in *N*,*N*′-dimethylformamide (DMF) solution, imidazolaledicarboxylate ligands generated in situ by complete hydrolysis of the cyano to carboxylate groups [3]. Twelve doubly deprotonated imidazolaledicarboxylate (HImDC) ligands

assemble with eight $In^{3+}$ metal ions forming the MOC, $[In_8(HImDC)_{12}]$. Each cube is connected via intermolecular hydrogen bonds between peripheral carboxyl and carboxylate groups with other cubes generating the porous network MOC-2 [1]. Moreover, Zhu et al. used 2-amino-4,5-dicyanoimidazole for synthesizing an amino-functionalized MOC-2 [4].

We obtained hydrogen-bonded metal–organic cubes with 4,5-dicyano-2-methoxyimidazole (L1) as ligand precursor [5–7]. The linker imidazolat-4,5-diamid-2-olate (L2) is formed in situ in the presence of a metal salt hydrate {$Zn(NO_3)_2{\cdot}4H_2O$, $(Co(NO_3)_2{\cdot}6H_2O$ and $Cd(ClO_4)_2{\cdot}6H_2O$} in DMF by partial hydrolysis of the cyano groups to amide groups and of the methoxy to the hydroxyl group followed by two-fold deprotonation (Scheme 1). Twelve ligands L2 assemble with fourteen metal ions ($Zn^{2+}$, $Co^{2+}$ and $Cd^{2+}$), an oxide ion, two hydroxide ions as well as four or eight solvent molecules (DMF, water) to cubic-like molecular building blocks (MBB) $[M_{14}(L2)_{12}(O)(OH)_2(S)_{4\text{ or }8}]$ (M = Zn, Co(II), Cd; S: solvent = $H_2O$ or DMF) with peripheral amide groups. The MBBs are connected with each other by intermolecular hydrogen bonds between the peripheral amide groups generating the porous supramolecular assemblies HIF-1, HIF-2 and HIF-3 (Scheme 1, HIF = Hydrogen-bonded Metal-Imidazolate Framework). By the reaction of L1 with $(Zn(NO_3)_2{\cdot}4H_2O$ and $(Co(NO_3)_2{\cdot}6H_2O$ in addition to HIF-1 [5] and HIF-2 [6], the metal–organic frameworks IFP-7 and IFP-8, respectively [IFP = Imidazolate Framework Potsdam)] are formed. IFP-7 and IFP-8 are the main products. In the case of HIF-3 [7], the MOF IFP-14 is the by-product.

Here, we varied various parameters for the syntheses of HIF-1 and HIF-2 to increase their yields and the crystallinity of the products. We found out that HIF-1 is generated in two different frameworks, named as HIF-1a and HIF-1b. The structure of HIF-1b is new and was solved by X-ray crystallography. We determined the gas sorption properties and the magnetism of HIF-2. Moreover, the UV/Vis-reflection spectra of HIF-1 (mixture of HIF1-a and b), HIF-2 and HIF-3 were measured.

## Results and discussion

### Syntheses

We repeated the syntheses of HIF-1 [5] and HIF-2 [6] by varying synthetic parameters. It revealed that the yields for both HIFs can be increased by increasing the solvent volume (DMF) and by the addition of seed crystals (cf. experimental part). Good crystallinities of HIF-1 and HIF-2 were obtained by a long cooling procedure already at higher temperatures in between 135 and 75 °C. To our surprise at these reaction conditions HIF-1 forms pale yellow crystals of different morphology, rhombic dodecahedrons and tetragonal elongated octahedrons. The dodecahedral crystals were isolated and characterized as ${}^3_\infty[Zn_{14}(L2)_{12}(O)(OH)_2(H_2O)_4]$ (HIF − 1) already earlier [5]. HIF − 2 $({}^3_\infty[Co_{14}(L2)_{12}(O)(OH)_2(DMF)_4])$ [6] forms deep purple colored crystals which have the same tetragonal elongated octahedral shape as the crystals we found now in addition to dodecahedral crystals at the synthesis of HIF-1. The IR data of the tetragonal elongated octahedral crystals generated at the HIF-1 synthesis are almost identical to that of HIF-2 (cf. experimental part). This was a further hint that we now isolated a HIF-1 framework which is isostructural to that of HIF-2. We named both HIF-1 frameworks HIF-1a (dodecahedral crystals) and HIF-1b (octahedral crystals), respectively (Scheme 1).

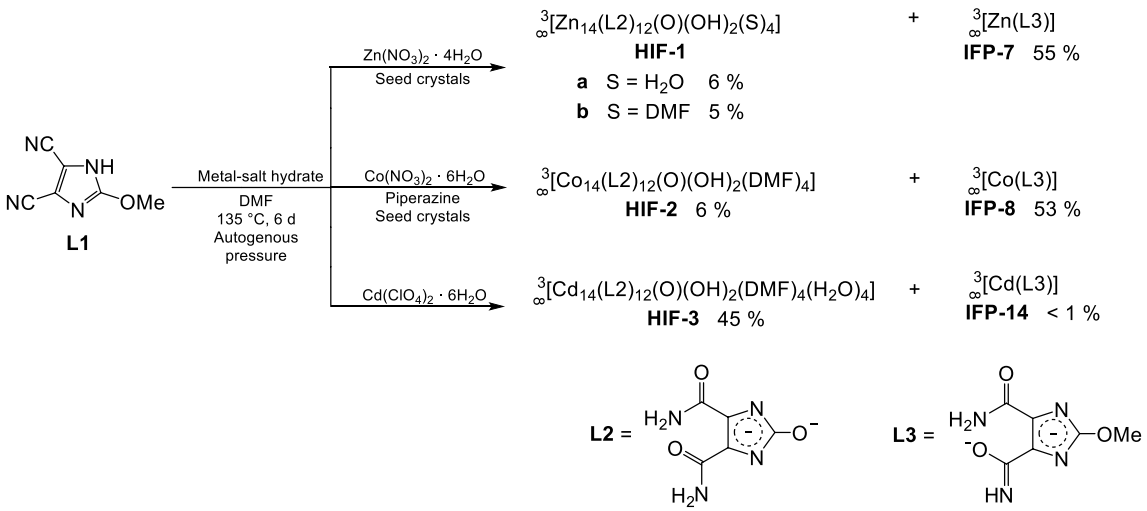


**Scheme 1** Syntheses of HIF-1a and b, HIF-2 and HIF-3

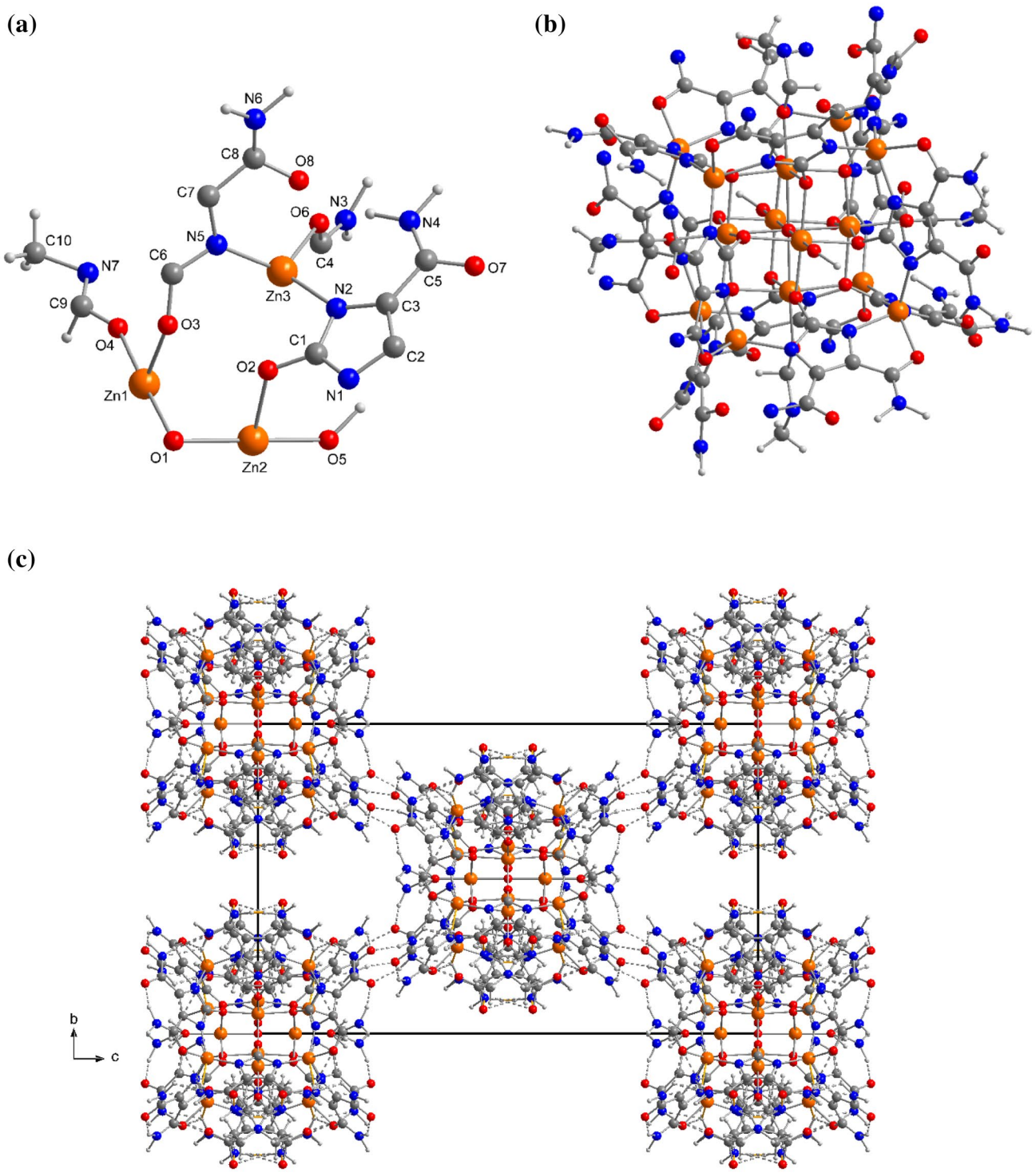


**Fig. 1** Crystal structure of HIF-1b: **a** asymmetric unit (without disordering), **b** tetradecanuclear zinc MBB ($[Zn_{14}(L2)_{12}(O)(OH)_2(DMF)_4]$) (hydrogen atoms are omitted for clarity), **c** hydrogen-bonded supramolecular assembly (orange Zn, blue N, red O, dark gray C, light gray H). (Color figure online)

## Crystal structures of HIF-1b

The single-crystal structure determination of HIF-1b confirmed our suspicion that this framework is an isostructural Zn homologue to HIF-2. The asymmetric unit of HIF-1b shows three different zinc centres (Zn1, Zn2 and Zn3) (Fig. 1a). At Zn1 DMF is coordinated. A MBB contains fourteen $Zn^{2+}$ ions (4 × Zn1, 2 × Zn2 and 8 × Zn3), twelve

ligands L2, an oxide ion, two hydroxide ions as well as four DMF ($[Zn_{14}(L2)_{12}(O)(OH)_2(DMF)_4]$) (Fig. 1b). Each MBB is connected vertex to vertex with eight MBBs by intermolecular N–H···O hydrogen bonds of peripheral amide groups generating the 3D supramolecular assembly HIF-1b (Fig. 1c). The difference of the structures of HIF-1b and HIF-1a are caused by the different coordinated solvent molecules. In a MBB of HIF-1b four DMF molecules are coordinated to four Zn1 centres ($[Zn_{14}(L2)_{12}(O)(OH)_2(DMF)_4]$) and in HIF-1a instead four coordinated water molecules are part of the MBB ($[Zn_{14}(L2)_{12}(O)(OH)_2(H_2O)_4]$) [5]. The solvent substitution of DMF for water lower the crystal symmetry of the HIF. Whereas HIF-1a crystallize in the space group $Ia\bar{3}d$ (No. 230) of the cubic crystal system, possessing the highest crystallographic symmetry, HIF-1b crystallize in the space group $I4/m$ (No. 87) of the tetragonal crystal system. Both frameworks, HIF-1a and HIF1b exhibit two types of infinite channels containing non-coordinated DMF and water molecules in the as-synthesized forms. But the solvent-accessible void volume in HIF-1a is almost equal than that in HIF-1b. It amounts for HIF-1a 53% and for HIF-1b 54.5%. The channels in HIF-1b show openings of 2.1 Å and 3.3 Å (see Figs. S3 and S4 in Supporting Information) and in HIF-1a of 3.9 Å and 6.0 Å [5]. The corresponding data for HIF-2, the isostructural Co homologue of HIF-1b, deviate only little from those of HIF-1b. For HIF-2, the solvent accessible void volume of 48% was determined and the openings of the channels amounts 1.7 Å and 3.2 Å [6].

The PXRD pattern of simulated HIF-1 and -3 exhibited the diffraction peaks closely matching with the as-synthesized samples (Fig. 2). However, the peak intensity of HIF-2 is very weak; only at $2\theta = 6$, a peak is observed. The remaining peaks at higher $2\theta$ values are broaden that might be the crystalline material became amorphous or unknown reasons. HIF-1b exhibits very good crystalline material among three HIFs. The PXRD pattern of IFP materials exhibited the diffraction peaks similar to that of the as-synthesized samples and their simulated patterns (Fig. 2). This indicates that the porous framework maintains the crystalline integrity and phase purity.

## Gas sorption of HIF-2

The channels of the as-synthesized HIF-2 contain solvent molecules (water and DMF). TGA measurement of as-synthesized HIF-2 indicated a loss of solvent molecules up to 200 °C based on a weight loss of 7% (Fig. 3). HIF-2 was activated at 120 °C heating and $10^{-4}$ mbar for 12 h. The activated sample of HIF-2 shows no decomposition below 250 °C. CoO is formed at 570 °C. Upon increasing the temperature, the mass increment is due to formation of $Co_3O_4$.

The nitrogen sorption isotherm of HIF-2 at 77 K presents a negligible nitrogen uptake (Fig. 4). To check if the nitrogen sorption is kinetically inhibited because of small pore size, hydrogen (at 77 K) and carbon dioxide (at 273 K) sorption isotherms were also collected. The latter two gases have a smaller kinetic diameter ($H_2$: 2.89 Å, $CO_2$: 3.3 Å) than $N_2$ (3.64 Å). In addition, at 273 K and under higher absolute pressures $CO_2$ molecules can more easily access ultramicropores than $N_2$ at ~ 77 K [8–10]. Still, the hydrogen sorption isotherm at 77 K shows also an essentially insignificant uptake to 8 $cm^3\ g^{-1}$. Also, the carbon dioxide sorption isotherm at 273 K presents only a small uptake of 13 $cm^3\ g^{-1}$. A tentative surface area calculation on the basis of the carbon dioxide uptake suggests a BET($CO_2$) surface area of 85 $m^2\ g^{-1}$. We note however, that this is close to the outer surface area of a fine powder which can be up to 50 $m^2\ g^{-1}$. Sorption measurements with methane revealed that this gas is not adsorbed by HIF-2. In comparison to HIF-1a (BET surface area of 471 $m^2\ g^{-1}$, $H_2$ uptake 95 $cm^3\ g^{-1}$, $CO_2$ uptake at 273 K 56 $cm^3\ g^{-1}$ [5]) HIF-2 possesses overall very low gas sorption uptakes. The reason for the very small gas uptakes in HIF-2 could be the smaller openings of the channels in HIF-2 of 1.7 Å and 3.2 Å compared to 3.9 Å and 6.0 Å in HIF-1a or a collapse of the framework upon activation as may be inferred from the comparison of the simulated and as-synthesized powder diffractograms of HIF-2 (Fig. 2a).

## Magnetic properties of HIF-2

HIF-2 contained paramagnetic cobalt(II) centres [6]. The question was how the cobalt(II) centres are interacting with each other, as it was mentioned before that the metal centers are bridged by oxide, hydroxide and linker.

The molecular building block of HIF-2 contains fourteen cobalt(II) centres. The cobalt atoms in the $Co_{14}$ cluster form a distorted $Co_8$ cube (Co3) with an inscribed $Co_6$ octahedron (Co1 and Co2) (Fig. 5a). The fourteen $Co^{2+}$ ions assemble with one oxide ion, twelve imidazolat-4,5-diamid-2-olate ligands L2, two hydroxide ions and four DMF molecules to the MBB. The oxide ion (O1) is located in the centre of the MBB, surrounded by four Co1 and two Co2 centres in an exact octahedral environment (Fig. 5b). The Co1 and Co2 centres are coordinated by six oxygen atoms in distorted octahedral coordination geometries (Fig. 5c). The four Co1 centres are surrounded in addition to the central oxide ion (O1) by four olate oxygen atoms (two O2 and two O3) and one DMF (O4). The two Co2 centres are coordinated by $O^{2-}$ (O1), four olate atoms (O2) and one hydroxide ion (O5). The remaining eight Co3 atoms are located above the eight triangle planes of the octahedron formed by the Co1 and Co2 centres. They are coordinated in a distorted tetrahedral coordination sphere by three nitrogen atoms (N1, N2 and N5) from two imidazolate ligands and an amide oxygen atom (O6). The tetrahedron is twofold

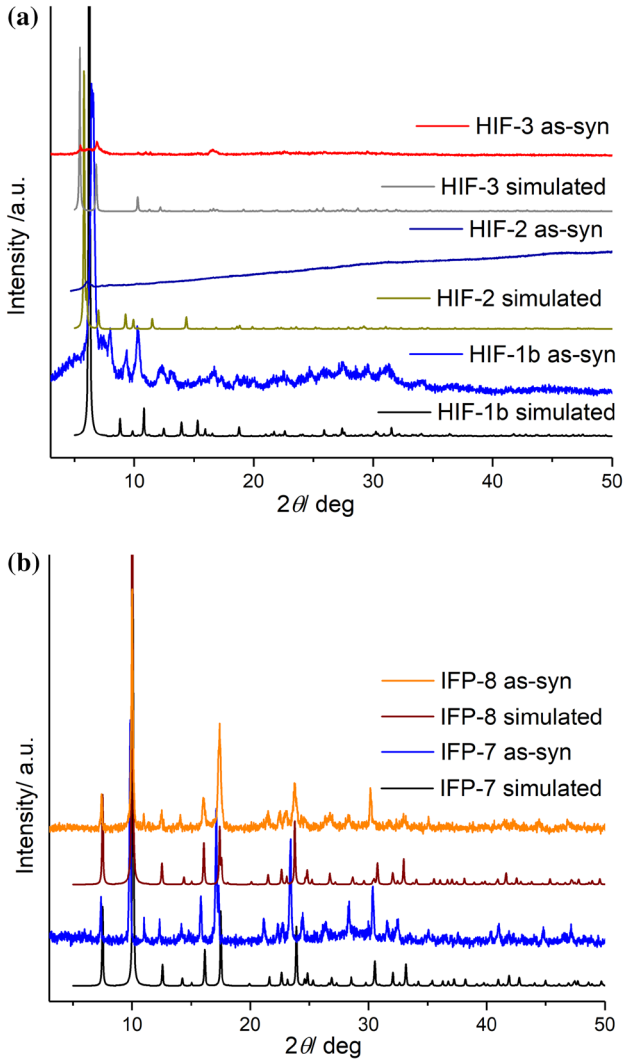


**Fig. 2** Powder X-ray diffraction patterns of **a** HIF and **b** IFP materials

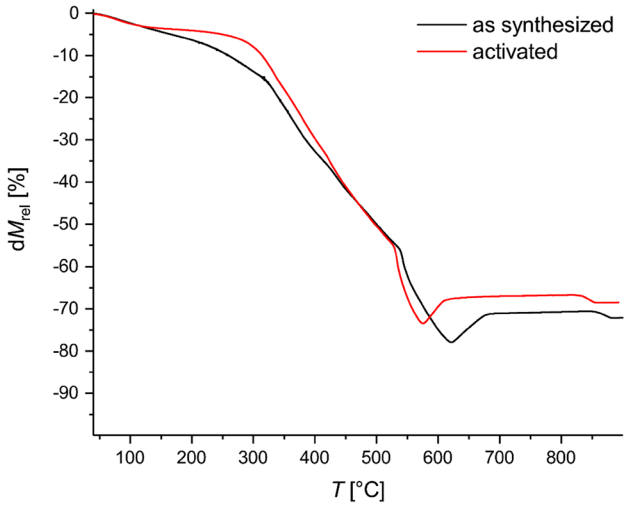


**Fig. 3** TGA curve of HIF-2 of an as-synthesized sample in comparison to an activated sample

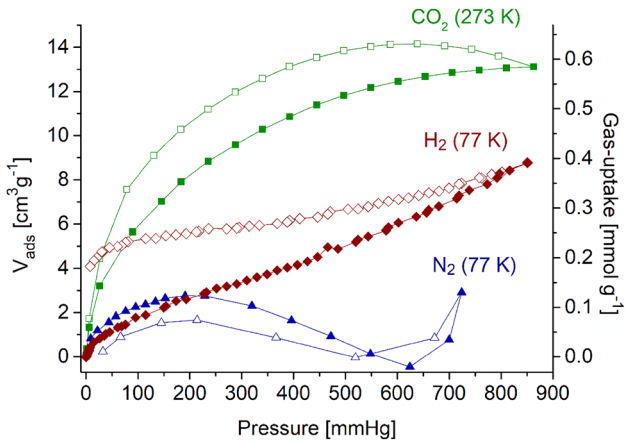


**Fig. 4** Gas sorption isotherms of HIF-2. Adsorption and desorption data points are indicated by filled and empty symbols, respectively

face-capped by one one olate atom (O2) and an amide atom (O8) at longer distances (2.9 Å and 2.5 Å, respectively) (Fig. 5c) [6].

Variable temperature magnetic susceptibility measurements were employed to investigate the magnetic behavior of HIF-2 over the temperature range from 2 to 300 K. Figure 6 shows $\chi_M T$ ($\chi_M$ = molar magnetic susceptibility) as a function of temperature $T$. At 300 K, the values for $\mu_{eff}$ ($\mu_{eff}$ = effective Bohr magneton number) and $\chi_M T$ amount to 15.94 $\mu_B$ and 31.74 cm$^3$ K mol$^{-1}$, respectively. The effective Bohr magneton number found is in good agreement with the calculated spin only value of $\mu_{SO} = 14.49\ \mu_B$ ($\chi_M T = 24.94$ cm$^3$ K mol$^{-1}$) four fourteen cobalt(II) high spin centres of the tetradecanuclear MBB of HIF-2. As the temperature is lowered, the values of $\chi_M T$ and $\mu_{eff}$ decrease, which indicates antiferromagnetic exchange interactions between the cobalt(II) centres. At 2 K, $\chi_M T$ ($\mu_{eff}$) tends to 1.34 cm$^3$ K mol$^{-1}$ (3.28 $\mu_B$), which implies almost full coupling of spins inside the tetradecanuclear cobalt(II) MBB.

In the temperature interval 50–300 K, the magnetic susceptibility obeys almost perfectly the Curie–Weiss law ($\chi = C/(T - \Theta)$) to give $C = 40$ cm$^3$ K mol$^{-1}$ and $\Theta = -76.4$ K (Fig. 7). The big negative Weiss constant indicates strong antiferromagnetic couplings between the cobalt(II) ions. The Néel-temperature ($T_N$) lies around 13 K.

Due to the size of the complex, only the magnetic properties of the octahedral core of the MBB were investigated. For the determination of the coupling constants between the inner cobalt atoms of the complex, a simplified model was considered: The L2 ligands were replaced by hydroxide ions and coordinated with water instead of DMF. The relative positions of the oxygen atoms correspond to the underlying

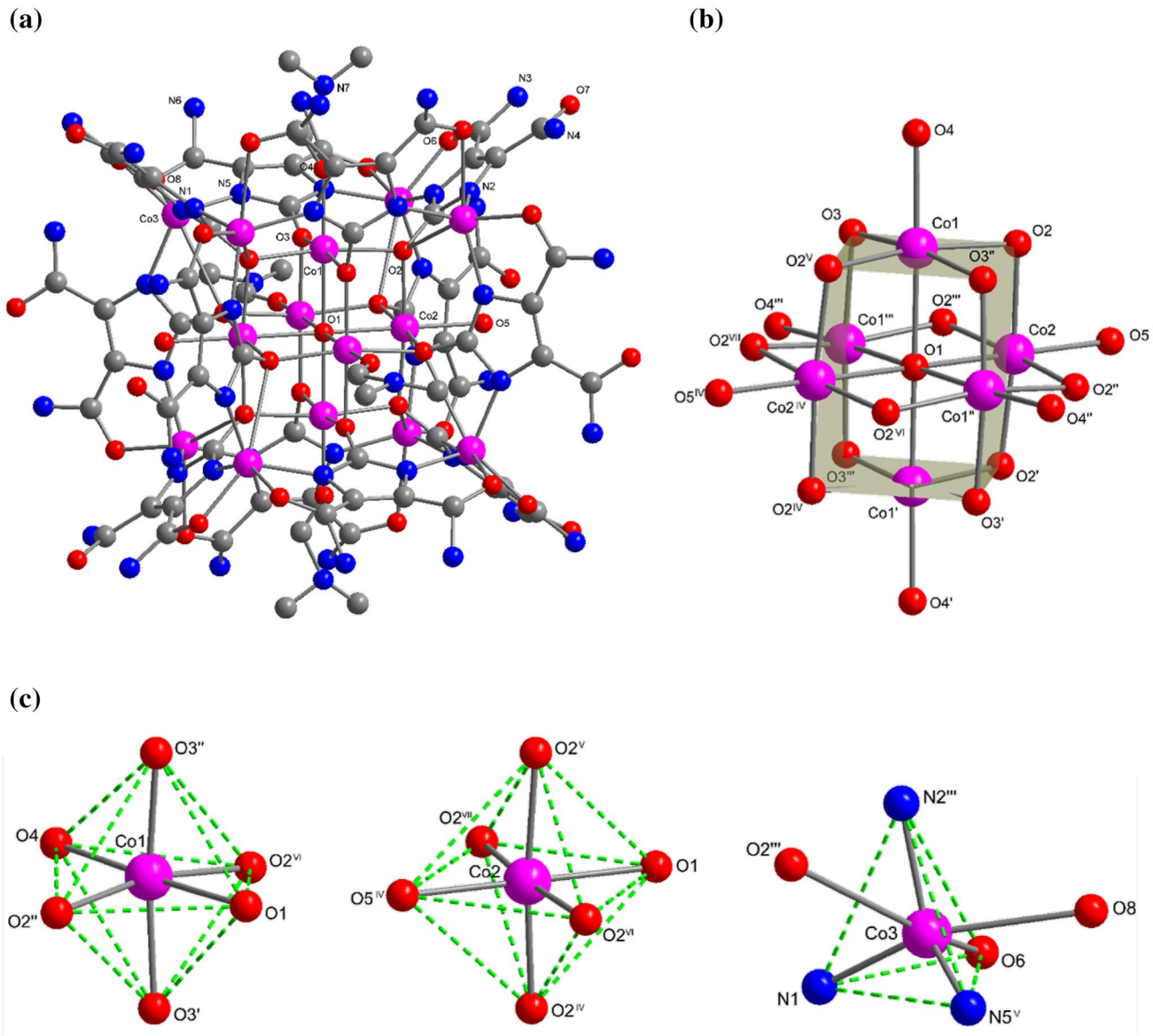


**Fig. 5** Cobalt(II) centres in HIF-2: **a** tetradecanuclear molecular building block, **b** central core of the MBB, **c** the coordination spheres of three cobalt(II) centres Co1, Co2 and Co3 (violet Co, blue N, red O, dark gray C, light gray H) [6]. (Color figure online)

crystal structure. The bond angles and bond lengths to the residual structures of L2 and DMF were retained during replacement by H atoms and only adapted for water to provide an additional bond (see Fig. 8 and Cartesian coordinates in the Supporting Information). The total charge of the model is − 4 such that the Co(II) nature of each metal centre is retained. The ligands ($H_2O$, $OH^-$, $O^{2-}$) lead, as L2, DMF and $OH^-$ in the full molecule, only to a small ligand field splitting, which is why the high spin state with a local spin of three unpaired electrons per cobalt centre was assumed for all cobalt ions.

The octahedron shown in Fig. 8 (right) is a schematic representation of the considered superexchange spin couplings between the different spin centers. The calculated coupling constants confirm the experimental results and suggest a consistently antiferromagnetic coupling character (see Table 1). However, a collinear alignment of the spins corresponding to these values is not possible for the structural arrangement under consideration, which suggests a spin-frustrated state. To minimize the likelihood of computational artifacts, we evaluated Heisenberg exchange coupling constants within Kohn–Sham density functional theory, employing two different exchange–correlation functionals. Both of them, B3LYP and TPSSh, show very similar trends.

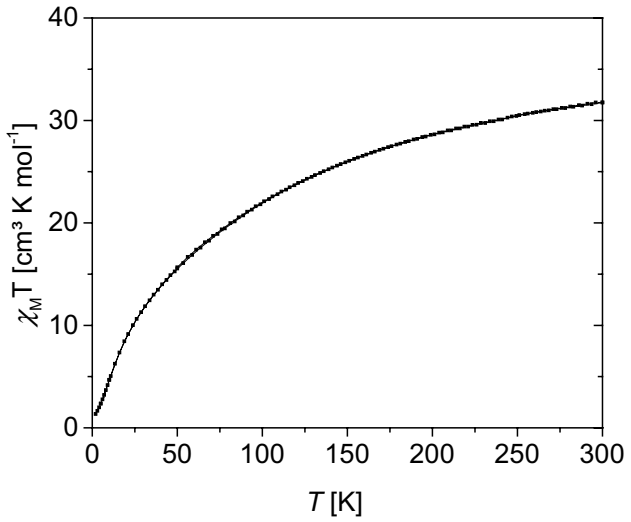


**Fig. 6** Variable temperature magnetic susceptibility measured from 2 to 300 K for HIF-2

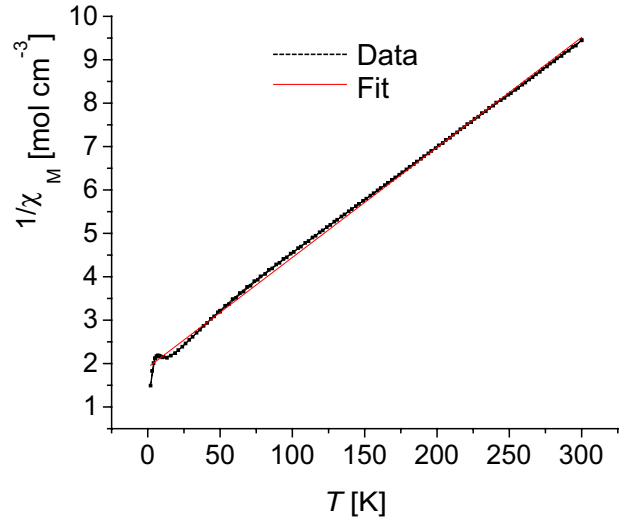


**Fig. 7** Curie plot of HIF-2

### UV/Vis spectroscopy

The UV/Vis diffuse reflectance spectra of the supramolecular hydrogen-bonded networks HIF-1 (mixture of HIF-1a and b), HIF-2 and HIF-3 as well as of the MOFs IFP-7 and IFP-8 (Fig. 9) showed similar absorption bands in the UV/Vis region between 280 and 450 nm, which corresponded to intra-ligand $\underline{n} \rightarrow \pi^*$ and $\pi \rightarrow \pi^*$ transition of imidazolate-4,5-diamid-2-olate L2 as well as of 2-methoxyimidazolate-4-amid-5-imidate L3. All three HIFs possessed a characteristic broad absorption band centered of imidazolate L2 around 340 nm. The corresponding absorption band of imidazolate L3 in the spectra of the IFPs IFP-7 and IFP-8, is observed between 310 and 320 nm. In the visible region, HIF-2 had a broad absorption band centered at 610 nm, which could be assigned to the spin-allowed d–d transition $^4A_2(F) \rightarrow {}^4T_2(P)$ of the tetrahedral Co3(II) ions (Fig. 5c) [12]. In the visible region, the Co(II)-IFP IFP-8 [6] show absorption bands assignable to the d–d transitions of the trigonal–bipyramidal five-coordinate high spin cobalt(II) ion [13]. HIF-1 and HIF-3 showed no detectable luminescence. One of the possibilities of luminescence is due to the outer sphere energy transfer that can also be negated as this type of buliding-block structure where the ligand is not coordinated extensively to other metal center.

## Conclusion

We showed the results of the syntheses of HIF-1 and HIF-2 obtained at different experimental conditions. It was found that the yields for both HIFs can be increased by increasing the solvent volume (DMF) and by the addition of seed crystals. The UV/Vis diffuse reflectance spectra of HIF-1 and HIF-2 showed a characteristic broad absorption band centered at 340 nm that corresponded to intra-ligand transition. In the visible region, HIF-2 had a broad absorption band centered at 610 nm assigned to d–d transitions of Co(II) ions. HIF-1 and HIF-2 are the by-products of solvothermal syntheses of IFP-7 and IFP-8, respectively. For their separation a relatively high yield and a good crystallinity is highly desirable. This can be achieved by increasing the solvent volume (DMF), by the addition of seed crystals and by a long cooling procedure already at higher temperatures in between 135 and 75 °C. At these reaction conditions, HIF-1 forms pale yellow crystals of different morphology, rhombic dodecahedrons (HIF-1a) and the up to now unknown tetragonal elongated octahedrons (HIF-1b). HIF-1b is isostructural to HIF-2, which crystallizes as deep purple colored tetragonal elongated octahedrons. In comparison to HIF-1a (BET surface area of 471 $m^2\ g^{-1}$), HIF-2 possesses very low gas sorption uptake properties. The reason could be the smaller openings of the channels in HIF-2 of 1.7 Å and 3.2 Å compared to 3.9 Å and 6.0 Å in HIF-1a. A tentative surface area calculation based on the carbon dioxide uptake revealed a BET($CO_2$) surface area of 85 $m^2\ g^{-1}$. The effective Bohr magneton number found at 300 K is in good agreement with the calculated spin only value four fourteen cobalt(II) high-spin paramagnetic centres of the tetradecanuclear MBB of HIF-2. As temperature lowers down, the values of $\chi_M T$ and $\mu_{eff}$ decrease, which indicates antiferromagnetic exchange interactions between the cobalt(II) centres. This is confirmed by Kohn–Sham density functional theory calculations.

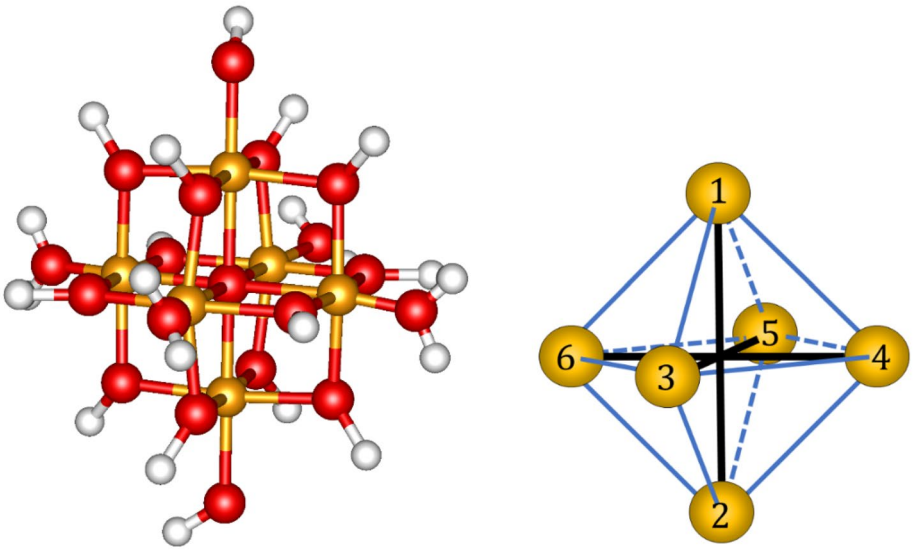


**Fig. 8** Model system for the $[Co_6(OR)_4(OR')_{12}(OH)_2]^{4-}$ core of the MBB (left) and polyeder representation of the considered couplings between the six spin centers (right)

**Table 1** Heisenberg exchange spin coupling constants J between the cobalt atoms of the reduced model system shown in Fig. 8, obtained from Kohn–Sham density functional theory with a def2-TZVP basis set and employing the exchange–correlation functionals B3LYP und TPSSh

| Coupling constant | B3LYP ($cm^{-1}$) | TPSSh ($cm^{-1}$) |
|---|---|---|
| **$J_1$(1, 2)** | − 18 | − 22 |
| **$J_2$(3, 5)** | − 12 | − 14 |
| **$J_3$(4, 6)** | − 10 | − 11 |
| $J_4$(5, 6) | − 7 | − 10 |
| $J_5$(3, 6) | − 7 | − 11 |
| $J_6$(3, 4) | − 3 | − 13 |
| $J_7$(4, 5) | − 10 | − 14 |
| $J_8$(1, 4) | − 2 | − 8 |
| $J_9$(2, 4) | − 5 | − 10 |
| $J_{10}$(2, 6) | − 5 | − 9 |
| $J_{11}$(1, 6) | − 3 | − 6 |
| $J_{12}$(1, 5) | − 7 | − 10 |
| $J_{13}$(1, 3) | − 3 | − 4 |
| $J_{14}$(2, 5) | − 7 | − 11 |
| $J_{15}$(2, 3) | − 5 | − 7 |

Coupling constants were obtained from a Green's function approach [11]

The values marked in bold-face are for pairs on the opposite corners of the Co octahedron

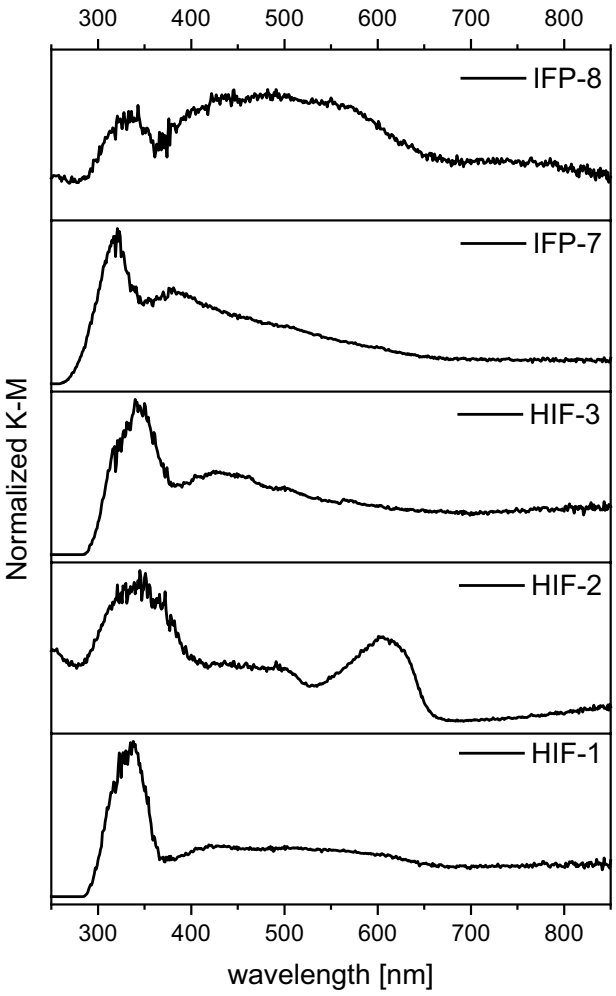


**Fig. 9** UV/Vis diffuse reflectance spectra (calculated via the Kubelka–Munk function and normalized for comparison) for HIF-1 (mixture of HIF-1a and b), HIF-2, HIF-3, IFP-7 and IFP-8

## Experimental

### Materials and methods

All reagents and solvents were used as purchased from commercial suppliers (Sigma-Aldrich, Fluka, Alfa Aesar,

and others) without further purification, if not stated otherwise. The linker precursor 4,5-dicyano-2-methoxyimidazole (L1) was synthesized following a published procedure [14].

## Syntheses

### HIF-1a and HIF-1b

In a sealed tube (TYP A, company: Ace) 4,5-dicyano-2-methoxyimidazole L1 (0.1 g, 0,68 mmol) and $Zn(NO_3)_2{\cdot}4H_2O$ (0.178 g, 0.68 mmol) were dissolved in DMF (7 ml) and some seed crystals are added. The sealed tube was closed and the mixture was heated at 135 °C for 6 days and was then allowed to cool very slowly to 75 °C during 12 h in steps of 5 °C per 30 min cooling and then 30 min waiting. Subsequently the reaction mixture was allowed to cool to room temperature overnight. Then the formed solids were separated from the reaction solution, washed with little DMF and tiped on filter paper. Under a microscope pale yellow crystals of dodecahedron morphology (HIF-1a, 0.009 g, 6%) as well as of elongated octahedron morphology (HIF-1b, 0.0075 g, 5%) could be separated from powdery IFP-7 by hand. IR (KBr pellet) of HIF-1b: $\nu_{max} = 3427, 3349, 1658, 1533, 1447, 1384, 1262, 1103, 758, 732, 692, 555, 494, 457\ cm^{-1}$.

### HIF-2

HIF-2 was prepared in a similar manner to that described for HIF-1a and HIF-1b using L1 (0.06 g, 0.41 mmol), $Co(NO_3)_2{\cdot}6H_2O$ (0.11 g, 0.38 mmol) and piperazine (0.02 g, 0.23 mmol) dissolved in DMF (4 ml). Deep purple colored tetragonal elongated octahedral crystals of HIF-2 (0.005 g, 6%) could be separated from powdery IFP-8. Co-elemental analysis (ICP-OES): calculated. for $[Co_{14}(L2)_{12}(O)(OH)_2(DMF)_4]$ 25.9%, exp. 22.8%. The divergence of 18.6% is caused by solvent molecules (DMF and $H_2O$) enclosed in the channels of HIF-2 as well as defects in the crystalline polymeric material. IR (KBr pellet): $\nu_{max} = 3426, 3344, 1659, 1529, 1444, 1384, 1254, 1102, 758, 729, 695, 555, 492, 459\ cm^{-1}$.

## IR spectra

IR spectra were recorded on FT-IR Nexus from Thermo Nicolet in the region of 4000–400 $cm^{-1}$ using KBr pellets.

## Powder X-ray-diffraction patterns

Powder X-ray diffraction (PXRD) patterns were measured on a Siemens diffractometer D5005 in Bragg–Brentano reflection geometry. The diffractometer was equipped with a copper tube, a scintillation counter, automatic incident- and diffracted-beam soller slits and a graphite secondary monochromator. The generator was set to 40 kV and 40 mA. All measurements were performed with sample rotation. Data were collected digitally from 3° to 70° $2\theta$ using a step size of 0.02° $2\theta$ and a count time of 4 s per step. The simulated powder patterns for framework materials were calculated using single-crystal X-ray diffraction data and processed by the free Mercury v1.4.2 program provided by the Cambridge Crystallographic Data Centre.

## Single-crystal structure determination of HIF-1b

A pale yellow elongated octahedron was embedded in perfluoropolyalkylether oil and mounted within a MicroGripper. For details of the data collection and the structure solution and refinement—see Supplementary Material. Crystal data $C_{8.5}H_{8.25}N_{6.5}O_{5.375}Zn_{1.75}{\cdot}2(C_3H_7NO)$, $M = 548.05$, tetragonal, space group $I4/m$, $a = b = 18.0657(4)$ Å, $c = 29.1202(8)$ Å, $V = 9503.9(5)$ Å$^3$, $Z = 16$, $D_C = 1.532$ g cm$^3$, $F(000) = 4484$, GOF = 0.976, $R_1 = 0.0587$ $(I > 2\sigma(I))$, $wR_2 = 0.1558$ (all data). CCDC-19011966 contains the supplementary crystallographic data for this paper. These data can be obtained free of charge from The Cambridge Crystallographic Data Centre via http://www.ccdc.cam.ac.uk/data_request/cif.

## Thermogravimetric (TG) analysis

TG measurements were performed in a static air atmosphere from room temperature up to 900 °C with a Perkin Elmer TGA 4000 thermal analyzer. The heating rate was 10 °C $min^{-1}$. The samples were placed in ceramic pans.

## Gas-sorption measurements

Sorption isotherms were measured using a Micromeritics ASAP 2020 automatic gas sorption analyzer equipped with oil-free vacuum pumps (ultimate vacuum $< 10^{-8}$ mbar) and valves, which guaranteed contamination free measurements. All used gases ($H_2$, He, $N_2$, $CO_2$) were of ultra-high purity (UHP, grade 5.0, 99.999%) and the STP volumes are given according to the NIST standards (293.15 K, 101.325 kPa). Helium gas was used for the determination of the cold and warm free space of the sample tubes. $H_2$ and $N_2$ sorption isotherms were measured at 77 K (liquid nitrogen bath), whereas the $CO_2$ sorption isotherm was measured at 273.15 K (ice/deionized water bath).

Before the first sorption experiment HIF-2 was activated at 120 °C under vaccum ($< 10^{-4}$ mbar) for 12 h. Due to a limited sample amount all experiments were performed with the same sample and measuring tube. In subsequent sorption

experiments the reused sample was activated for 3 h under same conditions.

### Magnetic susceptibility measurements

The magnetic susceptibility was measured using a SQUID MPMS-XL5 instrument from Quantum Design. A field of 0.5 T was applied over the temperature range. Gelatine capsules in a plastic straw were used for sample preparation. The diamagnetic parts of the sample holder and the organic ligand were corrected afterwards by using measured values and tabulated Pascal's constants [15].

### Theoretical analysis

The electronic structures were evaluated with the Gaussian09 program package [16] within Kohn–Sham density functional theory [17, 18]. Alrichs' def2-TZVP basis set [19, 20] along with the exchange correlation functionals B3LYP [21–26] and TPSSh [22, 23, 27] were used. The convergence criterion for the energy in the self-consistent field algorithm was set to $10^{-7}$ a.u. Heisenberg exchange spin coupling constants were calculated from a Green's function approach [11, 28–31] with the module JGreen [11, 29] of our program package Artaios [30].

### UV/Vis spectroscopy

The diffuse reflectance spectra were collected at a Lambda 750 (Perkin Elmer) UV/Vis spectrophotometer equipped with a 60 mm integrating sphere and by using Spectralon (labsphere, USRS-99-010, AS-01158-060) as reference. For each measurement an appropriate amount of substance was mixed with manganese sulphate ($MgSO_4$). This mixture was pressed to a pellet and placed into the sample holder of the spectrophotometer. The measured reflection data $R$ were converted into Kubelka–Munk $K$–$M$ values according to the Kubelka–Munk function

$$K-M = \frac{(1-R)^2}{2R}$$

**Acknowledgements** The authors thank Dr. J. Traeger and Ms. S. Lubahn (Universität Potsdam) for the ICP OES measurements.

## References

1. Guillerm, V., Kim, D., Eubank, J.F., Luebke, R., Liu, X., Adil, K., Lah, M.S., Eddaoudi, M.: A supramolecular building approach for the design and construction of metal-organic frameworks. Chem. Soc. Rev. **43**, 6141–6172 (2014)
2. Eddaoudi, M., Sava, D.F., Eubank, J.F., Adil, K., Guillerm, V.: Zeolite-like metal-organic frameworks (ZMOFs): design, synthesis, and properties. Chem. Soc. Rev. **44**, 228–249 (2015)
3. Sava, D.F., Kravtsov, V.C., Eckert, J., Eubank, J.F., Nouar, F., Eddaoudi, M.: Exceptional stability and high hydrogen uptake in hydrogen-bonded metal-organic cubes possessing ACO and AST zeolite-*like* topologies. J. Am. Chem. Soc. **131**, 10394–10396 (2009)
4. Guo, X.-Q., Wang, M., Meng, F., Tang, Y.-F., Tian, S., Yang, H.-L., Jiang, G.-Q., Zhu, J.-L.: Rational design and synthesis of an amino-functionalized hydrogen-bonded network with an ACO zeolite-like topology for gas storage. CrystEngComm **18**, 5616–5619 (2016)
5. Mondal, S.S., Bhunia, A., Kelling, A., Schilde, U., Janiak, C., Holdt, H.-J.: Giant $Zn_{14}$ molecular building block in hydrogen-bonded network with permanent porosity for gas uptake. J. Am. Chem. Soc. **136**, 44–47 (2014)
6. Mondal, S.S., Bhunia, A., Kelling, A., Schilde, U., Janiak, C., Holdt, H.-J.: A supramolecular $Co(II)_{14}$-metal-organic cube in a hydrogen-bonded network and a Co(II)-organic framework with a flexible methoxy substituent. Chem. Commun. **50**, 5441–5443 (2014)
7. Mondal, S.S., Dey, S., Attallah, A.G., Bhunia, A., Kelling, A., Schilde, U., Krause-Rehberg, R., Janiak, C., Holdt, H.-J.: Missing building blocks defects in a porous hydrogen-bonded amide-imidazolate network proven by positron annihilation lifetime spectroscopy. Chem. Sel. **1**, 4320–4325 (2016)
8. Bhunia, A., Boldog, I., Möller, A., Janiak, C.: Highly stable nanoporous covalent triazine-based frameworks with an adamantane core for carbon dioxide sorption and separation. J. Mater. Chem. A **1**, 14990–14999 (2013)
9. Mondal, S.S., Dey, S., Baburin, I.A., Kelling, A., Schilde, U., Seifert, G., Janiak, C., Holdt, H.-J.: Syntheses of two imidazolate-4-amide-5-imidate linker-based hexagonal metal-organic frameworks with flexible ethoxy substituent. CrystEngComm **15**, 9394–9399 (2013)
10. Mondal, S.S., Bhunia, A., Attallah, A.G., Matthes, P.R., Kelling, A., Schilde, U., Müller-Buschbaum, K., Krause-Rehberg, R., Janiak, C., Holdt, H.-J.: Study of the discrepancies between crystallographic porosity and guest access into cadmium-imidazolate framework and tunable luminescent properties by incorporation of lanthanides. Chem. Eur. J. **22**, 6905–6913 (2016)
11. Steenbock, T., Tasche, J., Lichtenstein, A.I., Herrmann, C.: A Green's-function approach to exchange spin coupling as a new tool for quantum chemistry. J. Chem. Theory Comput. **11**, 5651 (2015)
12. Leddver, A.B.P.: Inorganic Electronic Spectroscopy, p. 323. Elsevier, Amsterdam (1968)
13. Ciampolini, M., Nardi, N.: Complexes of bivalent iron, cobalt, nickel, and copper with bis(2-dimethylaminoethyl)oxide. Inorg. Chem. **6**, 445–449 (1967)
14. Anderson, W.K., Bhattacharjee, D., Houston, D.M.: Design, synthesis, antineoplastic activity, and chemical properties of bis(carbamate) derivatives of 4,5-bis(hydroxymethyl)-imidazole. J. Med. Chem. **32**, 119–127 (1989)
15. Kahn, O.: Molecular Magnetism. VCH, New York (1993)
16. Frisch, M.J., Trucks, G.W., Schlegel, H.B., Scuseria, G.E., Robb, M.A., Cheeseman, J.R., Scalmani, G., Barone, V., Mennucci, B., Petersson, G.A., Nakatsuji, H., Caricato, M., Li, X., Hratchian, H.P., Izmaylov, A.F., Bloino, J., Zheng, G., Sonnenberg, J.L., Hada, M., Ehara, M., Toyota, K., Fukuda, R., Hasegawa, J., Ishida, M., Nakajima, T., Honda, Y., Kitao, O., Nakai, H., Vreven, T., Montgomery Jr., J.A., Peralta, J.E., Ogliaro, F., Bearpark, M., Heyd, J.J., Brothers, E., Kudin, K.N., Staroverov, V.N., Kobayashi, R., Normand, J., Raghavachari, K., Rendell, A., Burant, J.C., Iyengar, S.S., Tomasi, J., Cossi, M., Rega, N., Millam, N.J., Klene, M., Knox, J.E., Cross, J.B., Bakken, V., Adamo, C., Jaramillo, J., Gomperts, R., Stratmann, R.E., Yazyev, O., Austin, A.J., Cammi, R., Pomelli, C., Ochterski, J.W., Martin, R.L., Morokuma, K.,

Zakrzewski, V.G., Voth, G.A., Salvador, P., Dannenberg, J.J., Dapprich, S., Daniels, A.D., Farkas, Ö., Foresman, J.B., Ortiz, J.V., Cioslowski, J., Fox, D.J.: Gaussian 09, Revision A.1. Gaussian Inc., Wallingford, CT (2009)
17. Parr, R.G., Yang, W.: Density-Functional Theory of Atoms and Molecules. Oxford University Press, New York (1989)
18. Cramer, C.J., Truhlar, D.G.: Density functional theory for transition metals and transition metal chemistry. Phys. Chem. Chem. Phys. **11**, 10757 (2019)
19. Weigend, F., Ahlrichs, R.: Balanced basis sets of split valence, triple zeta valence and quadruple zeta valence quality for H to Rn: design and assessment of accuracy. Phys. Chem. Chem. Phys. **7**, 3297–3305 (2005)
20. Weigend, F.: Accurate Coulomb-fitting basis sets for H to Rn. Phys. Chem. Chem. Phys. **8**, 1057–1065 (2006)
21. Becke, A.: Density-functional exchange-energy approximation with correct asymptotic behavior. Phys. Rev. A **38**, 3098 (1988)
22. Dirac, P.: Quantum mechanics of many-electron systems. Proc. R. Soc. A **123**, 714 (1929)
23. Slater, J.: A simplification of the Hartree–Fock method. Phys. Rev. **81**, 385 (1951)
24. Vosko, S., Wilk, L., Nusair, M.: Accurate spin-dependent electron liquid correlation energies for local spin density calculations: a critical analysis. Can. J. Phys. **58**, 1200 (1980)
25. Lee, C., Yang, W., Parr, R.: Development of the Colle–Salvetti correlation-energy formula into a functional of the electron density. Phys. Rev. B **37**, 785 (1988)
26. Becke, A.: Density-functional thermochemistry. III. The role of exact exchange. J. Chem. Phys. **98**, 5648–5652 (1993)
27. Perdew, J., Wang, Y.: Accurate and simple analytic representation of the electron-gas correlation energy. Phys. Rev. B. **45**, 1200 (1992)
28. Steenbock, T., Herrmann, C.: Towards an automated analysis of exchange pathways in spin-coupled systems. J. Comp. Chem. **39**, 81–92 (2018)
29. Deffner, M., Groß, L., Steenbock, T., Voigt, B. A., Solomon, G. C., Herrmann, C.: Artaios—a code for postprocessing quantum chemical electronic structure calculations. https://www.chemie.uni-hamburg.de/ac/herrmann/software/index.html (2008–2019)
30. Liechtenstein, A.I., Katsnelson, M.I., Gubanov, V.: Exchange interactions and spin-wave stiffness in ferromagnetic metals. J. Phys. F **14**, L125–L128 (1984)
31. Han, M., Ozaki, T., Yu, J.: Electronic structure, magnetic interactions, and the role of ligands in $Mn_n$(n = 4, 12) single-molecule magnets. Phys. Rev. B **70**, 184421 (2004)